JOURNAL OF COMPUTATIONAL PHYSICS 6, 510–526 (1970)

# A Lagrangian Method for Calculating Problems in Meteorology

Z. W. RITTER*

*National Center for Atmospheric Research,† Boulder, Colorado 80302*

Received April 13, 1970

A new method is presented for the numerical solution of some problems appearing in meteorology. The method is based on Lagrangian coordinates in contrast to other methods, which use the Eulerian representation. Lagrangian descriptions permit the accurate treatment of moving interfaces and free boundaries without using difficult interpolation schemes. Some examples illustrate the advantages of this new technique.

## 1. INTRODUCTION

Many different numerical methods have been developed for calculating the transient dynamics of incompressible fluids. A survey of different finite-difference schemes for the primitive equations for a barotropic fluid were given by Grammeltvedt in Ref. [1], who also cited in his paper a list of previous references.

All papers cited in Ref. [1] are based on the Eulerian concept of a fluid moving through a stationary network of cells and are most useful for problems involving large fluid distortions, as expected in meteorological problems.

Kasahara et al. [2] solved the problem of a moving cold front in the atmosphere, assuming a simplified mathematical model. His solution was also based on the Eulerian description. The motion of the free boundary, appearing in this problem, was calculated by using a special interpolation scheme [2].

Problems involving moving interfaces or complicated boundaries can be handled much more easily in a Lagrangian description of the moving fluids. The usefulness and the difficulties of the Lagrangian method are described in the literature in many different papers [3, 4]. We will briefly review some of the well-known facts.

A two-dimensional Lagrangian coordinate system that initially completely defines a system will often transform into one with areas of poor definition because of deformations of the grid during the motion of the fluid particles. Usually the trouble can be attributed to turbulence.

* On leave from The Scientific Department of the Ministry of Defense, P. O. Box 7063, Tel Aviv, Israel.

† The National Center for Atmospheric Research is sponsored by the National Science Foundation.

Another important feature, caused by the movement of the approximating grid with the fluid, is that the region describing the flow is always approximated by the same number of mesh points; thus the initial accuracy of the approximation is in general maintained throughout the calculation. Lagrange calculations have proven to be very accurate as long as the approximating mesh remains regular, and, in general, the number of mesh points needed is surprisingly small. Lagrange calculations are ideal in terms of accuracy and number of mesh points needed.

Unfortunately, the very features of the Lagrangian method which make it so useful are also the ones which make it totally unsatisfactory for calculating a flow in which turbulence develops. In such a case the mesh points will attempt to follow this motion and particles of mass which were initially nearest neighbors no longer remain so physically. The approximating mesh will become highly distorted, and the calculation becomes quite inaccurate if possible at all. In such situations the time interval required for stability tends to approach zero because the time interval needed for stability is proportional to the shortest distance separating two grid points. The minimum distance between two neighbors will tend to approach zero when the mesh becomes distorted.

These would appear to be the reasons why Lagrangian description was not used in meteorology. The expected deformation of a Lagrangian grid as described by Welander [8] is tremendous.

## 2. Basic Equations for The Calculated Models

Two problems were investigated in order to test the usefulness of the Lagrangian description in meteorology. The first (Problem A) had been solved by Grammeltvedt [1], Williamson [6], and Houghton et al. [5]. The second (Problem B) had been solved by Kasahara et al. [2].

In Problem A we calculated the motion of a barotropic fluid with a free surface. The hydrostatic fluid is incompressible, homogeneous, inviscid, and confined in a channel corresponding to a middle latitude band on the earth. The lower surface is flat and rigid, but the upper surface is free.

The basic equations for this model in Lagrangian form are

$$u_t = f \cdot v - g \cdot \frac{1}{A}(h_j y_k - h_k y_j), \tag{1}$$

$$v_t = -f \cdot u + g \cdot \frac{1}{A}(h_j x_k - h_k x_j), \tag{2}$$

$$x_t = u, \tag{3}$$

$$y_t = v, \tag{4}$$

$$(hA)_t = 0, \tag{5}$$

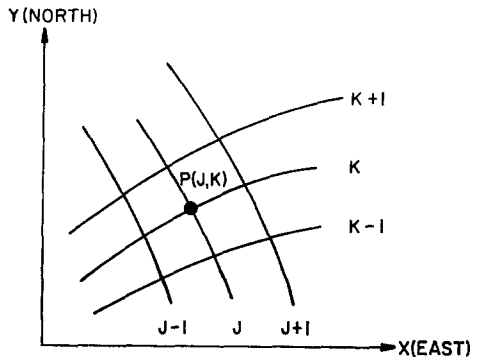


FIG. 1. Lagrangian coordinate network $(j, k)$.

where

$x, y$ are the Eulerian Cartesian, east–west and north–south coordinates,

$u, v$ are the velocity components in the $x$ and $y$ directions,

$h$ is the depth of the fluid,

$A = (x_j y_k - x_k y_j)$ is the Jacobian of transformation,

$f$ is the Coriolis parameter,

$g$ is the acceleration of gravity.

All functions are dependent on the Lagrangian labels $(j, k)$ and the time $t$. $x = x(j, k, t)$; $y = y(j, k, t)$; etc. Equations (1, 2) are the momentum equations in Lagrangian description, and Eq. (5) expresses the conservation of mass. The equation for total energy (potential plus kinetic) integrated over the channel is

$$E = \int_\sigma \int \tfrac{1}{2}(u^2 + v^2 + gh)\, h\, d\sigma, \tag{6}$$

where

$\sigma$ = area of integration.

In Problem B we calculated the motion of a cold air front in the atmosphere using the same assumptions as described by Kasahara et al. [2]. After making the simplifications assumed by Kasahara, one gets a set of partial differential equations very similar to those described in Problem A. The three dependent variables are two horizontal velocity components and the height of the cold air layer; the three independent variables are two space coordinates and time. Using an Eulerian description, Kasahara et al. [2] had to overcome a special numerical difficulty which arises because the moving front is a free boundary along which the differential equations are, in a certain sense, singular. They developed a special interpolation

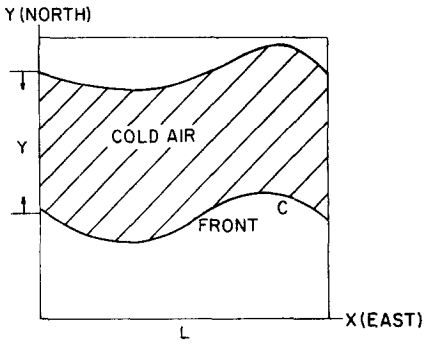


FIG. 2. The domain of numerical integration.

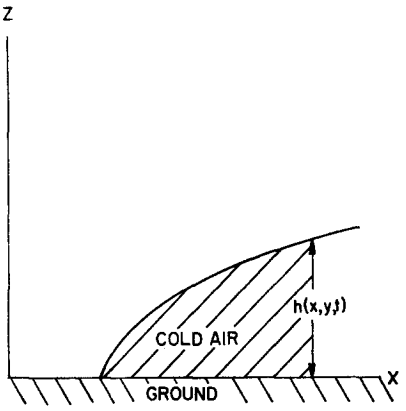


FIG. 3. Vertical cross section of the cold air layer.

scheme to calculate the motion of the front points [2] in every time step. After carrying out the numerical calculations over a large enough time interval they obtained the asymmetric shape of the moving front, developed from an initially sinusoidal pattern. Such a development was predicted qualitatively by Stoker [7], and this phenomenon also has actually been observed in nature.

Figures 2 and 3 show the initial state of the dynamic system. The cold air is bounded by the curve $C$ (Fig. 2), along which the height $h$ of the cold air is zero during the entire time. Figure 3 is a vertical cross section of the cold air layer.

We were able to reproduce the results of Ref. [2] without interpolation by using the moving front as a part of a Lagrangian grid and solving the following equations of motion:

$$u_t = f \cdot v - G \cdot \frac{1}{A}(h_j y_k - h_k y_j), \tag{7}$$

$$v_t = -f \cdot u + F + G \cdot \frac{1}{A}(h_j x_k - h_k x_j), \tag{8}$$

$$x_t = u, \tag{9}$$

$$y_t = v, \tag{10}$$

$$(hA)_t = 0. \tag{11}$$

All the symbols have the same meaning as before [Eqs. (1–5)]. Additional symbols are

$$G = g\left(1 - \frac{\rho'}{\rho}\right),$$

$$F = f \cdot \frac{\rho'}{\rho} \cdot \bar{u}',$$

where $\rho, \rho'$ are the densities of the cold and warm air, respectively, and $\bar{u}'$ is a given constant velocity. The essential difference now is, of course, the moving southern boundary $C$ describing the motion of the cold air front.

## 3. Boundary and Initial Conditions

In Problem A rigid boundaries were assumed along two latitude circles. The northern and southern boundaries, 4500 km apart, are rigid walls at which the normal velocity components vanish. The flow is assumed to be periodic in the east–west direction, with a wavelength of 6000 km. A $\beta$-plane approximation is used.

The height of the free surface is given initially, and the velocity components $u$ and $v$ are calculated from the geostrophic approximation.

We tested our method for three different initial conditions, as given in Ref. [1],

$$h^{(i)}(x, y) = H_0 + H_1 \tanh\left(\frac{9(y - y_0)}{2D}\right) + H_2 \operatorname{sech}^2\left(\frac{9(y - y_0)}{D}\right) \cdot f^{(i)}(x), \tag{12}$$

$$i = 1, 2, 3,$$

$$i = 1: \quad f^{(1)}(x) = \sin\left(\frac{2\pi x}{L}\right), \tag{A/I}$$

$$i = 2: \quad f^{(2)}(x) = \left[0.7 \sin\left(\frac{2\pi x}{L}\right) + 0.6 \sin\left(\frac{6\pi x}{L}\right)\right], \tag{A/II}$$

$$i = 3: \quad f^{(3)}(x) = \left[0.8 \sin\left(\frac{2\pi x}{L}\right) + 0.5 \sin\left(\frac{12\pi x}{L}\right)\right], \tag{A/III}$$

where $L$ is the length, $D$ is the width, and $y_0 = D/2$ is the middle latitude of the channel.

In the numerical calculations the following values are adopted:

$$H_0 = 2000 \text{ m}, \quad g = 10 \text{ m} \cdot \text{sec}^{-2}, \quad f = 10^{-4} \text{ sec}^{-1},$$
$$H_1 = -220 \text{ m}, \quad L = 6000 \text{ km}, \quad \beta = 1.5 \cdot 10^{-11} \text{ sec}^{-1} \cdot m^{-1},$$
$$H_2 = 133 \text{ m}, \quad D = 4500 \text{ km}.$$

In Problem B we assumed that $u$, $v$, and $h$ are periodic in the space variable $x$ with a period equal to the distance $L$ between the east and west boundaries. The motion of the northern boundary was calculated using the simple assumption that the velocities of the boundary points are equal to the velocities of their neighbors. The southern boundary, which describes the moving front, is defined as a line along which $h = 0$ the entire time. Assuming the height in the row outside this moving boundary to be equal to minus the height in the last row inside the boundary assures that the height along the moving front always remains zero.

The calculations were performed for both initial conditions given in Ref. [2],

$$h^{(1)}(x, y) = \frac{f}{G}\left(\frac{\rho'}{\rho}\bar{u}' - \bar{u}\right)(y - y_c(x)) \quad \text{for} \quad \bar{Y}^{(1)}(x) \geqslant y \geqslant y_c(x),$$

$$\frac{\rho'}{\rho}\bar{u}' > \bar{u}(\bar{u}' = \text{constant}),$$

$$y_c(x) = C_1 \sin\left(\frac{2\pi}{L}x - \frac{\pi}{2}\right) + C_2,$$

$$\bar{Y}^{(1)}(x) = y_c(x) + Y,$$

$$u(x, y) = \bar{u} = \text{constant},$$

$$v(x, y) = 0, \tag{B/I}$$

$$h^{(2)}(x, y) = h^{(1)}(x, y) \cdot \frac{\bar{Y}^{(2)} - b}{\bar{Y}^{(2)} - y_c(x)} \quad \text{for} \quad \bar{Y}^{(1)}(x) \geqslant y \geqslant y_c(x),$$

$$b = C_1 + C_2, \quad \bar{Y}^{(2)} = Y + C_2 - C_1,$$

$$\left.\begin{aligned} u(x, y) &= -\frac{G}{f}\frac{\partial h^{(2)}}{\partial y} + \frac{\rho'}{\rho}\bar{u}' \\ v(x, y) &= \frac{G}{f}\frac{\partial h^{(2)}}{\partial x} \end{aligned}\right\} \text{geostrophic assumption.} \tag{B/II}$$

The numerical values adopted were

$$L = 5 \cdot 10^6 \text{ ft} = 1.524 \cdot 10^6 \text{ m},$$

$$Y = 5 \cdot 10^6 \text{ ft} = 1.524 \cdot 10^6 \text{ m},$$

$$C_1 = 5 \cdot 10^5 \text{ ft} = 1.524 \cdot 10^5 \text{ m},$$

$$C_2 = 23.75 \cdot 10^5 \text{ ft} = 7.239 \cdot 10^5 \text{ m},$$

$$g = 32.1521 \text{ ft} \cdot \text{sec}^{-2} = 9.80 \text{ m} \cdot \text{sec}^{-2}$$

$$f = 10^{-4} \text{ sec}^{-1},$$

$$\bar{u} = 10 \text{ ft} \cdot \text{sec}^{-1} = 3.048 \text{ m} \cdot \text{sec}^{-1},$$

$$\frac{\rho'}{\rho}\bar{u}' = 50 \text{ ft} \cdot \text{sec}^{-1} = 15.24 \text{ m} \cdot \text{sec}^{-1},$$

$$G = g\left(1 - \frac{\rho'}{\rho}\right) = 0.6 \text{ ft} \cdot \text{sec}^{-2} = 0.18288 \text{ m} \cdot \text{sec}^{-2}.$$

## 4. Finite Difference Scheme and The Problem of Stability

The functions $x$, $y$, $u$, and $v$ are defined at the vertices $x(j, k)$, $y(j, k)$ of the quadrilateral cells of the Lagrangian grid; heights for the center of each cell, $h(j + \frac{1}{2}, k + \frac{1}{2})$, and also areas $A$ (Fig. 4) are stored.

The quantities stored for the cells and their vertices are advanced in time through small time steps, $\Delta t$. In each cycle the new values of the velocities are first calculated, then the vertices are moved to new positions. Using the new positions one calculates the new areas. Finally, using conservation of mass, one is able to calculate the new heights and to complete the cycle,

$$\begin{aligned}
u(j, k, n+1) &= \bar{u}(j, k, n) + \Delta t \cdot A^x(j, k, n), \\
v(j, k, n+1) &= \bar{v}(j, k, n) + \Delta t \cdot A^y(j, k, n), \\
x(j, k, n+1) &= x(j, k, n) + \Delta t \cdot u(j, k, n), \\
y(j, k, n+1) &= y(j, k, n) + \Delta t \cdot v(j, k, n), \\
[hA](j + \tfrac{1}{2}, k + \tfrac{1}{2}, n+1) &= [hA](j + \tfrac{1}{2}, k + \tfrac{1}{2}, n),
\end{aligned} \tag{13}$$

where $A$ is the area of the quadrilateral whose vertices are at (1, 2, 3, 4) (Fig. 4), and $A^x$, $A^y$ are the accelerations in the $x$ and $y$ directions.

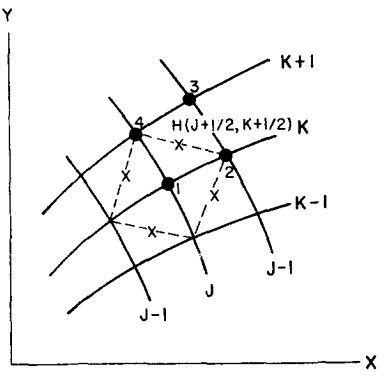


FIG. 4. Finite difference scheme.

Explicit difference approximations for the accelerations $A^x(j, k, n)$ and $A^y(j, k, n)$ are given in the Appendix as they appear in the literature [3, 4],

$$\bar{u}(j, k, n) = \alpha \cdot \bar{u}(j, k, n) + (1 - \alpha)\, u(j, k, n),$$
$$\bar{v}(j, k, n) = \alpha \cdot \bar{v}(j, k, n) + (1 - \alpha)\, v(j, k, n), \tag{14}$$
$$\bar{u}(j, k, n) = \tfrac{1}{4}[u(j + 1, k) + u(j - 1, k) + u(j, k + 1) + u(j, k - 1)],$$
$$\bar{v}(j, k, n) = \tfrac{1}{4}[v(j + 1, k) + v(j - 1, k) + v(j, k + 1) + v(j, k - 1)],$$
$$0 \leqslant \alpha \leqslant 1. \tag{15}$$

In order to stabilize the finite difference scheme it is necessary to use some kind of "artificial viscosity." In analogy to the well-known Lax–Wendroff method, we found that we could accomplish this by using an average velocity of $\bar{u}$, $\bar{v}$ in the momentum equation. For $\alpha = 0$, the set is unstable; for $\alpha = 1$, the set is super-stable; after some time all points are moving with the same velocity. We found that $\alpha = 0.02$ made our set stable as long as the deformation of the grid was not too great.

The criteria for choosing the time step are based on two assumptions. First, it is obvious that in a Lagrangian description a vertex should not be moved during one time step so far that it crosses over a neighboring vertex. As long as the deformations of the grid caused by physical reasons are not too big, the calculations are possible and meaningful.

The second assumption is based on the well-known Courant–Levy criterion, which in our case may be expressed by

$$\Delta t < \min \left( \frac{A(j, k)}{u^2(j, k) + v^2(j, k) + gh(j, k)} \right)^{1/2} \cdot C_0, \tag{16}$$

where

$A(j, k)$ is the area of the quadrilateral,

$u$, $v$ are the velocities of the fluid,

$(gh)^{1/2}$ is the velocity of gravity waves,

$C_0$ = constant $\approx 0.1$.

## 5. Results of The Calculations

The set of equations describing Problem A was integrated with initial conditions A/I, A/II, and A/III until instability occurred. Using a basic grid of $16 \times 12$ gridpoints corresponding to a grid size of 400 km in the west–east and south–north directions, respectively, we were able to continue our calculations for four days; the time step used, 60 sec, remained constant. After four days the deformations of the grid were growing because of the inherent turbulence of the fluid, and finally after six days no meaningful calculation was possible. By using smaller time steps it was possible to continue the calculations for physically longer times, but the deformations of the grid still finally became too great, pointing out that this result reflects the physical reality of the problem.

We were unable to stabilize our equations for a longer time by adding to the momentum equations a term containing viscosity [4] and by using reasonable values for the kinematic viscosity $\nu$.

Some examples of our results are given in Fig. 5. Figures 5a, b show the Lagrangian grid and the height field at time $T = 0$. Figures 5c–f show the grid and the height field after one and three days of integration using initial conditions A/I. Calculations based on initial conditions A/II and A/III essentially gave the same results.

All our calculated results, as well as those published in previous papers [1, 5, 6], depend still on the number of grid points and on the time step used. In order to get a numerical solution converging to the exact solution of the problem, it is necessary to use a much denser grid and therefore also much more computing time. Our calculations were sufficient to convince us that a Lagrangian description is applicable, at least for short range numerical weather prediction.

Problem B was integrated for both initial conditions B/I and B/II. The Lagrangian grid used in this case is formed initially by sinusoidal lines parallel to the moving front (lines with $k$ = constant) and by lines parallel to the direction of the $y$ axes (lines with $j$ = constant), Fig. 6. All calculations were performed over 21 grid points (20 intervals) in both directions and with a time step $\Delta t = 30$ sec. The moving front points are a part of the grid from the very beginning, and their motion is calculated in just the same way as all the other points of the fluid,

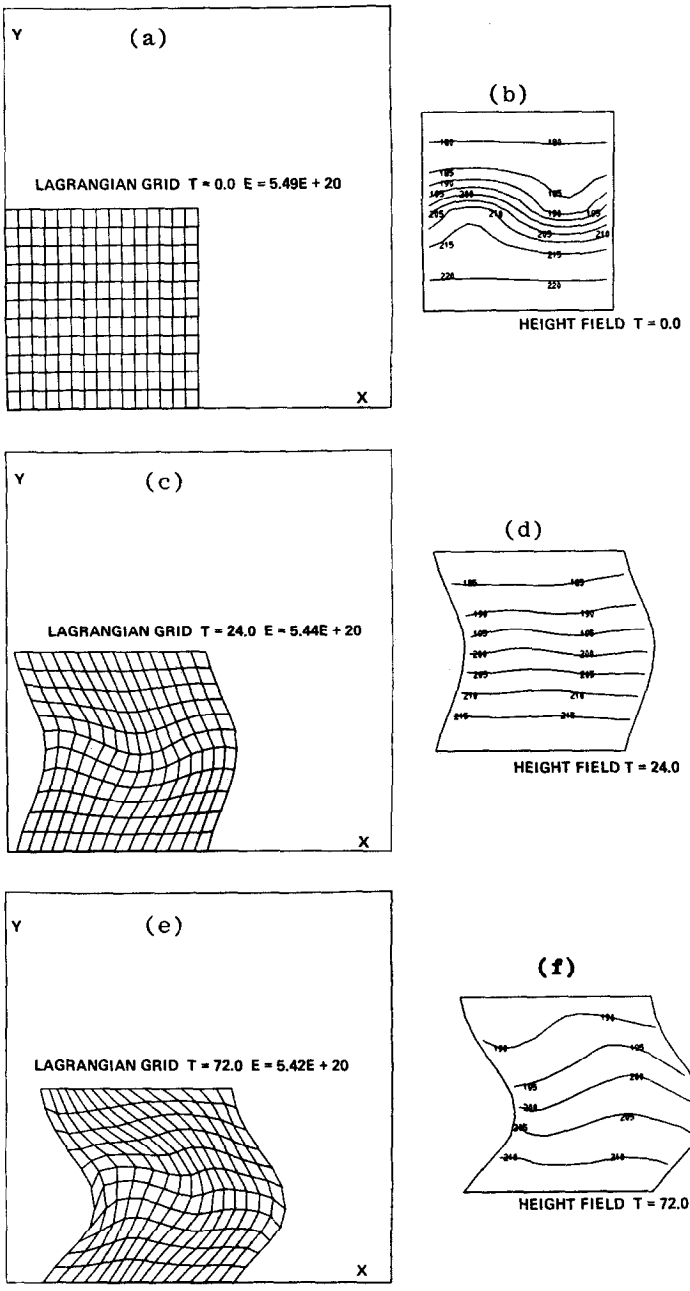


FIG. 5. The motion of a barotropic fluid (Case A/I). The height contour lines are shown at 50 m intervals. (a) Lagrangian grid $T = 0$; (b) height field $T = 0$; (c) Lagrangian grid $T = 24$ hr; (d) height field $T = 24$ hr; (e) Lagrangian grid $T = 72$ hr; (f) height field $T = 72$ hr.

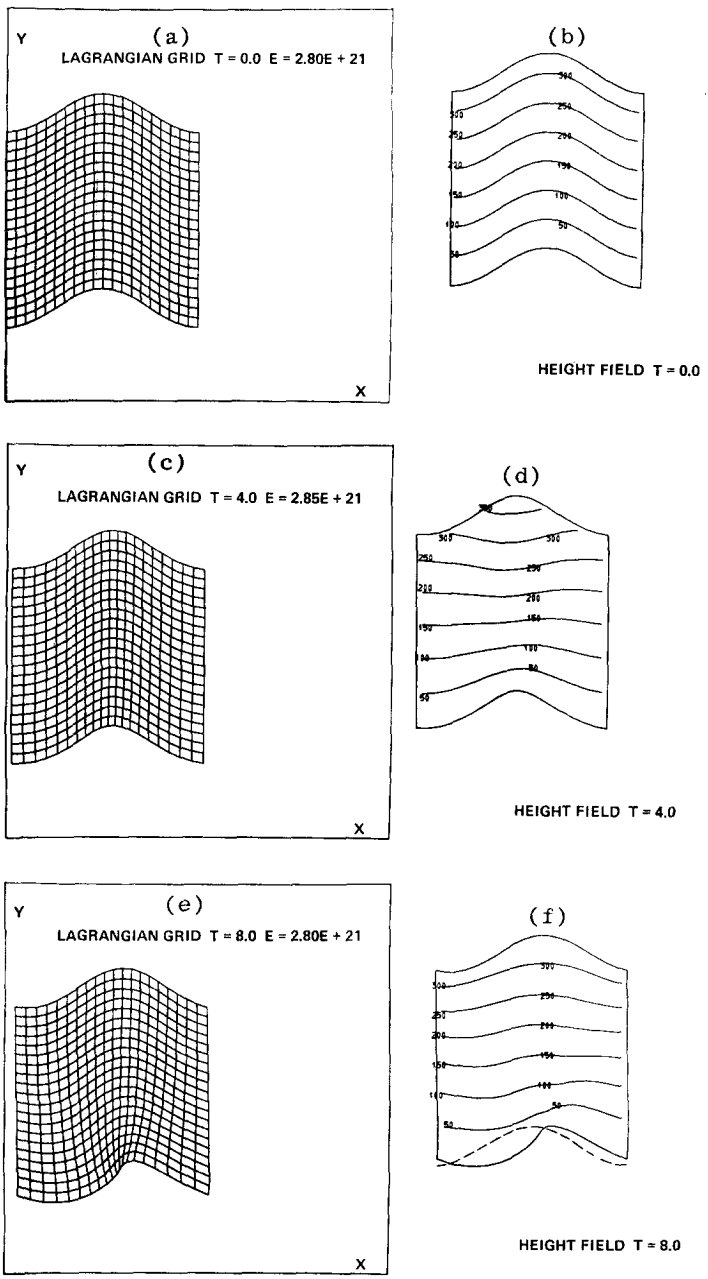


FIG. 6. The moving front (Case B/I). The height contour lines are drawn at 5000 ft intervals. (a) Lagrangian grid $T = 0$; (b) height field $T = 0$; (c) Lagrangian grid $T = 4$ hr; (d) height field $T = 4$ hr; (e) Lagrangian grid $T = 8$ hr; (f) height field $T = 8$ hr.

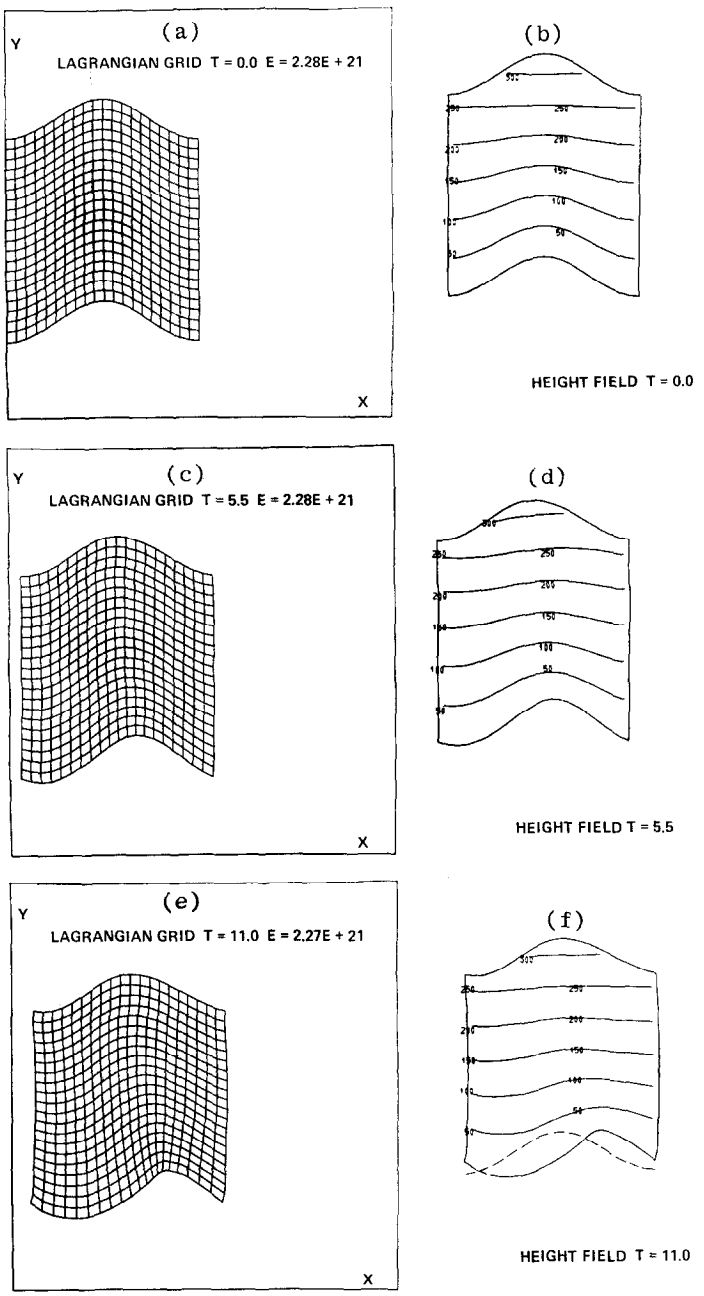


FIG. 7. The moving front (Case B/II). The height contour lines are drawn at 5000 ft intervals. (a) Lagrangian grid $T = 0$; (b) height field $T = 0$; (c) Lagrangian grid $T = 5.5$ hr; (d) height field $T = 5.5$ hr; (e) Lagrangian grid $T = 11$ hr; (f) height field $T = 11$ hr.

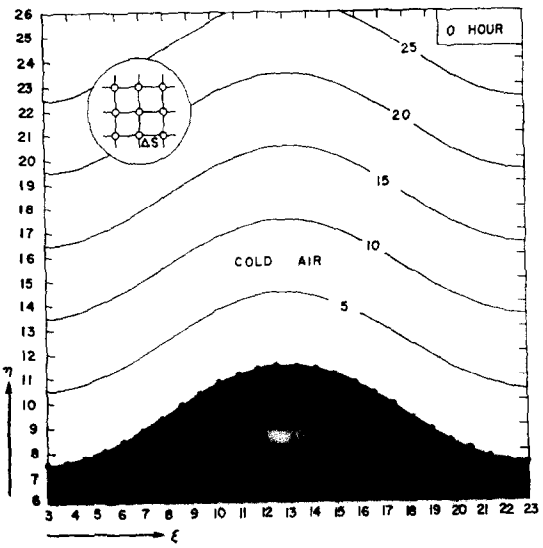


FIG. 8. Height contour pattern of cold air for Case A at $t = 0$. The contour lines are drawn at 5000 ft intervals. (Reprinted from Ref. [2].)

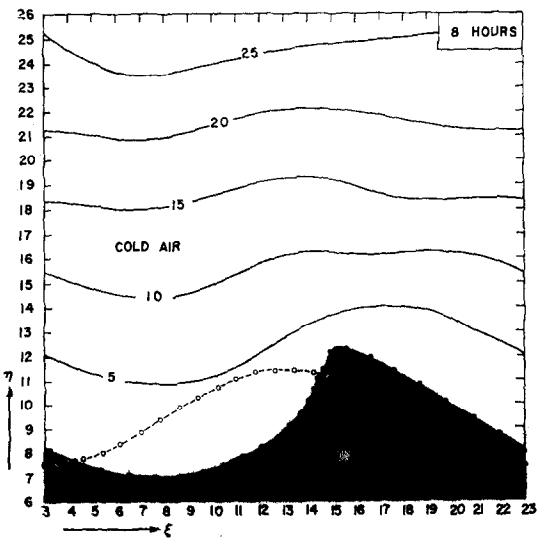


FIG. 9. Height contour pattern of cold air for Case A at $t = 8$ hr. The contour lines are drawn at 5000 ft intervals. (Reprinted from Ref. [2].)

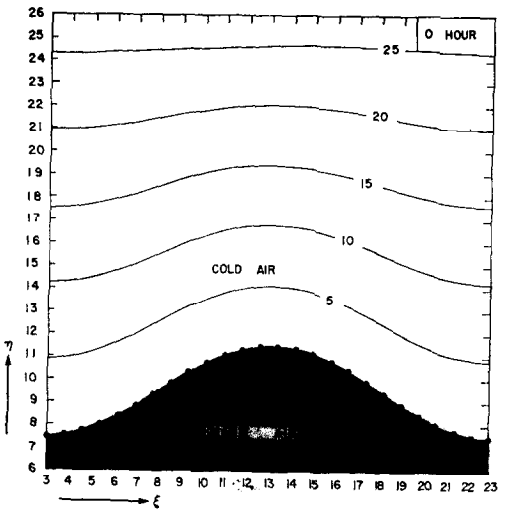


FIG. 10. Height contour pattern of cold air for Case B at $t = 0$, similar to Fig. 8. (Reprinted from Ref. [2].)

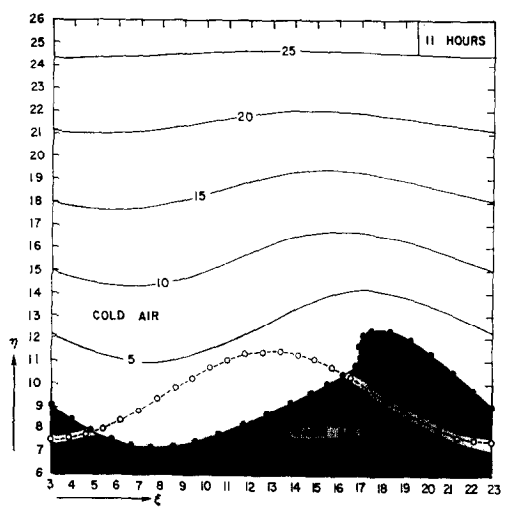


FIG. 11. Height contour pattern of cold air for Case B at $t = 11$ hr, similar to Fig. 9. (Re. printed from Ref. [2].)

always using the boundary condition $h = 0$. In Figs. 6a, b we show the initial form of the grid and the height contour pattern of the cold air for initial conditions B/I. The contour lines $h$ = constant are drawn at 5000 ft intervals. The front points are given by $k = 1$ for all $j$ values. Figures 6c–f show the grid points and the contour pattern of the cold air height at $T = 4$ h and 8 h. The location of the initial curve of the front, corresponding to a uniform translation in the $x$ direction, is indicated by the dashed line in Fig. 6f.

The entire front progressed eastward. The cold front moved eastward faster than the warm front, and the characteristic asymmetry is clearly visible. Points on the cold front moved southeastward, and those on the warm front moved northwestward on the average, whereas both fronts themselves propagated eastward.

The result is essentially the same as that calculated by Kasahara et al. [2]. Because of our special choice of this Lagrangian grid, we were able to reproduce their results without any interpolation procedure. The necessary computing time on the Control Data 6600 was 140 sec.

Our results, based on initial conditions B/II, are shown in Fig. 7. The initial form of the grid and the height contour pattern of the cold air are shown in Figs. 7a, b, which are similar to Figs. 6a, b. But in this case the initial wind field is geostrophic in both directions. The slope of the height of the cold air is constant in the $y$ direction but variable with respect to the $x$ direction. Figures 7c–f show the grid points and the contour pattern of the cold air height at $T = 5.5$ hr and 11 hr. Just as before, it was again observed that the entire front system progressed eastward and the characteristic assymetry was again clearly visible after 11 hr (Fig. 7f). In order to compare our results with that previously calculated in Ref. [2], we reproduced, with the permission of the authors, some figures of their paper. Their Figs. 8–9 correspond to our Fig. 6 and their Figs. 10–11 to our Fig. 7.

The total mass of the moving air is automatically conserved in a Lagrangian description, and the total energy of the system is approximately constant in both cases with a variation of less than 1 % during the whole integration time.

## 6. Conclusions

This paper represents a first step in the development of a new numerical method for calculating the transient dynamics of hydrostatic incompressible fluids. The method uses Lagrangian coordinates, which make the treatment of moving boundaries and material interfaces straightforward.

The new method is illustrated by some test calculations that establish its validity and usefulness. In general, it is most suited for problems not undergoing large distortions but requiring an accurate knowledge of moving fluid boundaries.

## APPENDIX

Detailed difference equations for the acceleration terms are written out in this appendix. The equations are for interior vertices and cells. The necessary changes at the different boundaries are described in Section 3.

$$A^x(j,k) = \frac{g}{2A(j,k)}\,(H(j+\tfrac{1}{2},k+\tfrac{1}{2})[Y(j+1,k)-Y(j,k+1)] + H(j-\tfrac{1}{2},k+\tfrac{1}{2})[Y(j,k+1)-Y(j-1,k)] + H(j-\tfrac{1}{2},k-\tfrac{1}{2}) \cdot [Y(j-1,k)-Y(j,k-1)] + H(j+\tfrac{1}{2},k-\tfrac{1}{2})[Y(j,k-1)-Y(j+1,k)]) + \frac{f}{4}[V(j+1,k)+V(j-1,k)+V(j,k+1)+V(j,k-1)] \cdot R(j,k), \tag{A.1}$$

where

$$A(j,k) = \tfrac{1}{4}[A(j+\tfrac{1}{2},k+\tfrac{1}{2}) + A(j+\tfrac{1}{2},k-\tfrac{1}{2}) + A(j-\tfrac{1}{2},k+\tfrac{1}{2}) + A(j-\tfrac{1}{2},k-\tfrac{1}{2})], \tag{A.2}$$

$$R(j,k) = \frac{1}{8A(j,k)}\,([Y(j,k+1)-Y(j+1,k)][X(j+1,k+1)-X(j,k)+X(j+1,k)-X(j,k+1)] + [Y(j,k+1)-Y(j-1,k)][X(j,k+1)-X(j-1,k)+X(j,k)-X(j-1,k+1)] + [Y(j-1,k)-Y(j,k-1)] \cdot [X(j,k)-X(j-1,k-1)+X(j,k-1)-X(j-1,k)] + [Y(j+1,k)-Y(j,k-1)][X(j+1,k)-X(j,k-1)+X(j+1,k-1)-X(j,k)]), \tag{A.3}$$

and similar expressions for $A^y(j,k)$,

$$A^y(j,k) = \frac{g}{2A(j,k)}\,(H(j+\tfrac{1}{2},k+\tfrac{1}{2})[X(j,k+1)-X(j+1,k)] + H(j-\tfrac{1}{2},k+\tfrac{1}{2})[X(j-1,k)-X(j,k+1)] + H(j-\tfrac{1}{2},k-\tfrac{1}{2}) \cdot [X(j,k-1)-X(j-1,k)] + H(j+\tfrac{1}{2},k-\tfrac{1}{2})[X(j+1,k)-X(j,k-1)]) - \frac{f}{4}[U(j+1,k)+U(j-1,k)+U(j,k+1)+U(j,k-1)] \cdot Q(j,k), \tag{A.4}$$

where

$$
\begin{aligned}
&Q(j,k)\\
&\quad=\frac{1}{8A(j,k)}\,([X(j+1,k)-X(j,k+1)][Y(j,k+1)-Y(j+1,k)\\
&\qquad+Y(j+1,k+1)-Y(j,k)]+[X(j,k+1)-X(j-1,k)][Y(j,k+1)\\
&\qquad-Y(j-1,k)+Y(j-1,k+1)-Y(j,k)]+[X(j,k-1)-X(j-1,k)]\\
&\qquad\cdot[Y(j-1,k)-Y(j,k-1)+Y(j,k)-Y(j-1,k-1)]+[X(j+1,k)\\
&\qquad-X(j,k-1)][Y(j+1,k)-Y(j,k-1)+Y(j,k)-Y(j+1,k-1)]).
\end{aligned}
\tag{A.5}
$$

The area $A(j+\frac{1}{2},k+\frac{1}{2})$ is calculated as the sum of two determinants (Fig. 4),

$$
A(j+\tfrac{1}{2},k+\tfrac{1}{2})=\tfrac{1}{2}\left[\begin{vmatrix} X(2), & Y(2), & 1\\ X(3), & Y(3), & 1\\ X(4), & Y(4), & 1\end{vmatrix}+\begin{vmatrix} X(2), & Y(2), & 1\\ X(4), & Y(4), & 1\\ X(1), & Y(1), & 1\end{vmatrix}\right]. \tag{A.6}
$$

## ACKNOWLEDGMENTS

The author is very indebted to B. Haurwitz and P. D. Thompson, of the NCAR Advanced. Study Program, for their generous hospitality in providing the stimulating environment in which this work was carried out and for enabling him to use the Control Data 6600 computer to perform the necessary computations. He would also like to thank A. Kasahara and D. Williamson of the NCAR Laboratory of Atmospheric Science for many useful discussions and D. Robertson for his aid in using different plotting routines. The author is also indebted to Prof. R. D. Richtmyer of the University of Colorado Mathematics Department for his careful reading and valuable criticism of the manuscript. Finally, the author wishes to express his gratitude to the Scientific Department of the Ministry of Defense in Israel for financial assistance which made his research trip to the United States possible.

## REFERENCES

1. A. GRAMMELTVEDT, *Mon. Weather Rev.* **97** (1969), 384.
2. A. KASAHARA, E. ISAACSON AND J. J. STOKER, *Tellus* **17** (1965), 261.
3. Methods in Computational Physics, (B. ALDER, S. FERNBACH, AND M. ROTENBERG, Eds.), Vol. 3, Academic Press, New York, 1964.
4. C. W. HIRT, J. J. COOK, AND T. D. BUTLER, Los Alamos Scientific Lab., Rep. LA-DC-10584.
5. D. HOUGHTON, A. KASAHARA, AND W. WASHINGTON, *Mon. Weather Rev.* **94** (1966), 141.
6. D. WILLIAMSON, NCAR Manuscript 68-169 (1968).
7. J. J. STOKER, "Water Waves," Chapter 10, Interscience, New York, 1957.
8. P. WELANDER, *Tellus* **7** (1955), 141.